Restricted – Commercial *Contract Report*

EC Contract No.: FIGM-CT-2000-20078

Deliverable No. D5 (Work Package 5)

NRPB-PE/1/2004

Assessment of Patient Dose in CT

P C Shrimpton

Assessment of Patient Dose in CT

P C Shrimpton

ABSTRACT

This report summarises work undertaken in support of a European Commission (EC) Concerted Action on CT that has included both a review and further development of the framework for CT dosimetry. The system previously established by the EC for reference doses in CT (with the quantities *weighted CTDI ($CTDI_w$)* and *dose-length product (DLP)*) has been expanded to include subsequent developments in CT technology, such as multi-slice scanners and the recommendation for display of *volume CTDI ($CTDI_{vol}$)* on the scanner console. New Monte Carlo calculations for CT have been carried out to supplement the relative lack of normalised organ dose data available for paediatric patients. Series of simulations have been completed for 3 particular models of scanner and 6 mathematical phantoms representing ages newborn, 1y, 5y, 10y, 15y and adult. Analysis of these results has confirmed the trends for an enhancement of the doses to small children relative to those to adults under similar conditions of CT exposure, by factors up to 2.6 in the case of the newborn patient, depending on scanner model and region of scan. A new comprehensive framework is proposed for assessing organ doses in CT based on coefficients relating them to corresponding values of $CTDI_w$ in the standard (head or body) CT dosimetry phantoms. This approach would potentially provide a single set of dose coefficients for each standard patient age for universal application to all scanner models. Some initial values are presented of effective dose normalised both to $CTDI_w$ and *DLP* for combinations of standard examination and phantom age.

This study was partially funded by the European Commission under Contract No FIGM-CT-2000-2078.

Chilton
Didcot
Oxon OX11 0RQ

Approval: March 2004
Publication: March 2004

CONTENTS

1 INTRODUCTION

Over a lifetime of presently some thirty years, x-ray computed tomography (CT) has matured into an indispensable tool for the diagnosis and management of disease and pathology (Golding and Shrimpton, 2002). Patient doses have remained relatively high in comparison with those for many other x-ray procedures and, accordingly, CT is necessarily an important topic in the radiological protection of patients (ICRP, 2000; UNSCEAR, 2000). Guidelines to promote good practice in CT were initially established by the European Commission (EC) under the 4th Framework Research Programme (Shrimpton, 1997) and, after review and revision (Shrimpton, 1999), finally published in 1999, with recommendations concerning both the quality of clinical images and also radiation dose (European Commission, 1999). Continuing advances in technology and clinical application, particularly in relation to paediatric CT, have prompted the revision of these quality criteria under the EC 5th Framework Research Programme (Contract No. FIGM-CT-2000-20078).

This report presents a summary of the review and further development of CT dosimetry undertaken by NRPB as part of this Contract.

2 ESTABLISHED FRAMEWORK FOR CT DOSIMETRY

Dosimetry is an essential requirement for optimisation of patient protection in CT. There is a need not only to estimate typical organ doses and risks to patients from CT procedures, but also to conduct periodic monitoring to evaluate the effectiveness of patient protection as part of routine quality assurance (Shrimpton, 2002). Appropriate dose quantities and methods for such dosimetry are discussed below.

2.1 Organ and effective doses

The direct measurement of organ dose for patients undergoing CT is impractical for most organs. Comprehensive dose assessment in CT necessarily involves the simulation of clinical practice using physical or mathematical representations of the patient (anthropomorphic phantoms), together with direct measurement or computational modelling of the dose distribution (ICRP, 2000; UNSCEAR, 2000).

In particular, Monte Carlo calculations for specific models of CT scanner have already provided coefficients that facilitate the estimation of organ and effective doses for CT examinations (McCollough, 2000). One of the most widely-used sets of systematic data is that based on simulations carried out at NRPB (Jones and Shrimpton, 1991) and published as software report NRPB-SR250 (Jones and Shrimpton, 1993). This provides tabulations of organ dose coefficients, normalised to a free-in-air axial dose, for the irradiation of each of 208

contiguous 5 mm transverse slabs of an adult geometric mathematical phantom. Additional software is required (e.g. Le Heron, 1993) for manipulation of these data in order to estimate doses for particular scanning protocols. The NRPB report provides 23 sets of data relating to a range of conditions of exposure relevant to 27 scanner models (from 5 manufacturers) that were current during the early 1990s. When normalised to axial air kerma, values of effective dose calculated for a standard anatomical region vary by up to a factor of three between data sets (Shrimpton and Edyvean, 1998).

Most of the scanner models included in the report NRPB-SR250 have long since been superseded, although broad methods for the matching of new scanner models to existing data sets have been developed on the pragmatic basis of measurements in standard CT dosimetry phantoms (European Commission, 1999; ImPACT, 2003). However, whereas the ImPACT dosimetry spreadsheet in particular has usefully extended the utility of NRPB-SR250 in the short term, such scanner matching remains very approximate since it considers only effective dose calculated for broad anatomical regions of the adult mathematical phantom relative to practical measurements of the computed tomography dose index, CTDI (Leitz et al, 1995). Data sets matched in this way may not provide reliable estimates of organ dose or effective dose from more specific CT examinations for a new scanner. Moreover, the data sets refer to the adult mathematical phantom and so can not be used directly for paediatric CT.

Another key source of dose coefficients for CT examinations are the Monte Carlo calculations carried out at GSF, Munich (Zankl et al, 1991). These data also refer to 3 obsolete models of scanner, although application of the results to other scanners has been elaborated (Kalender et al, 1999; Nagel, 2002). Monte Carlo calculations for CT have also been reported by Wise (1994), Jansen et al (1996), Baadegaard and Jensen (1999), Alonso et al (2002) and Jarry et al (2003).

Methods of computational dosimetry continue to advance with the development of more realistic (voxel) mathematical phantoms based on digital images of humans (Petoussi-Henss et al, 2002). Differences in the dose to a given organ from calculations for different anthropomorphic phantoms under similar conditions of exposure serve to highlight the uncertainties and limitations in such computed dose coefficients. Results determined for standard phantoms should not be applied to examinations of individual patients, although patient-specific computational modelling is now possible (Schmidt and Kalender, 2002).

Organ dose coefficients relevant to paediatric CT have, until recently, been limited to specific data for a few voxel or physical phantoms, pending completion of further Monte Carlo calculations at NRPB for a complete family of 6 geometric mathematical phantoms representing standard patients of ages from newborn to adult (Khursheed et al, 2002; this publication is reproduced in Appendix A). These data are discussed further in Section 3 below.

2.2 Energy imparted

An alternative approach to CT dosimetry focuses on the energy imparted to the patient as a practical measure of patient dose (Huda and Atherton, 1995). Whereas this method does not provide information about the doses to individual organs, it nevertheless allows a broad assessment of risk and the estimation of effective doses (Atherton and Huda, 1996). In particular, considerations of energy imparted provided an early assessment of the increased effective doses to paediatric patients relative to those for adults under similar CT scan conditions (Huda et al, 1997). Further such studies have demonstrated trends in dose with patient size for CT examinations of the thorax (Huda et al, 2000), abdomen (Huda, Scalzetti and Levin, 2001) and head (Huda et al, 2001).

2.3 Reference dosimetry

Notwithstanding the need for some assessment of organ and effective dose, there is also a requirement for periodic dose monitoring using simpler and more practical dose quantities to characterise local performance as part of routine quality assurance. In general, wide-scale surveys of dose have indicated significant variations in performance between hospitals and led to the development of quantitative guidelines on patient dose as ways of promoting good practice (Wall and Shrimpton, 1998). In particular, the concept of diagnostic reference doses (DRLs) is now recognised internationally as a useful and practical tool for facilitating optimisation of patient protection (ICRP, 1996; IAEA, 1996). Indeed, the formal use of DRLs is mandatory for Member States of the European Union (European Commission, 1997) through implementation in national legislation (eg IRMER, 2000).

A robust methodology for the specific reference dosimetry necessary for CT has already been developed by the European Commission, initially in relation to examinations on adult patients (European Commission, 1999), and with subsequent application to paediatric CT (Shrimpton and Wall, 2000).

The principal dosimetric quantity used in CT is the CT dose index (CTDI). This is defined as the integral along a line parallel to the axis of rotation (z) of the dose profile (D(z)) for a single rotation and a fixed table position, divided by the nominal thickness of the x-ray beam. CTDI can be conveniently assessed using a pencil ionisation chamber with an active length of 100 mm, so as to provide a measurement of $CTDI_{100}$, expressed in terms of absorbed dose to air (IEC, 2003; IPEM, 2003):

$$CTDI_{100} = \frac{1}{N \times T} \int_{-50}^{+50} D(z)dz \qquad \text{(mGy)} \qquad (1)$$

where N is the number of tomographic sections, each of nominal thickness T (mm), from a single rotation. For multi-slice CT scanners, where N > 1, NxT

(mm) represents the total detector acquisition width (eg 4 x 5 mm), and is equivalent to the nominal beam collimation.

Reference dosimetry for CT is based on such measurements made within standard CT dosimetry phantoms; these presently comprise homogeneous cylinders of polymethylmethacrylate (PMMA), with diameters of 16 cm (adult head) and 32 cm (adult body). The combination of measurements made at the centre (c) and 10 mm below the surface (p) of a phantom leads to the following reference dose quantities (European Commission, 1999) which can be applied to serial or spiral scanning, for both single- or multi-slice geometry scanners.

2.3.1 Weighted CT dose index ($CTDI_w$)

The weighted CTDI in the standard adult head or body CT dosimetry phantom for a single rotation corresponding to the exposure settings used in clinical practice is defined as:

$$CTDI_w = \frac{1}{3} CTDI_{100,c} + \frac{2}{3} CTDI_{100,p} \quad \text{(mGy)} \quad (2)$$

where $CTDI_{100,p}$ represents an average of measurements at four equally-spaced locations around the periphery of the phantom.

Monitoring of $CTDI_w$ per rotation takes account of the exposure settings selected, such as tube current and tube voltage.

2.3.2 Volume weighted CT dose index ($CTDI_{vol}$)

The volume weighted CTDI has been defined by the International Electrotechnical Commission (2003):

$$CTDI_{vol} = \frac{CTDI_w}{CT\ pitch\ factor} \quad \text{(mGy)} \quad (3)$$

where

$$CT\ pitch\ factor = \frac{\Delta d}{N \times T} \quad (4)$$

and Δd is the distance (mm) moved by the patient support in the z-direction between consecutive serial scans or per rotation in helical scanning; NxT (mm) is the nominal beam collimation (Equation 1). $CTDI_{vol}$ is recommended for display on the CT scanner console (IEC, 2003).

$CTDI_{vol}$ represents the average value of the weighted CTDI throughout the volume scanned in a particular sequence.

2.3.3 Dose-length product (DLP)

The dose-length product (DLP) for a complete examination is defined as:

$$DLP = \sum_i {}_nCTDI_W \times (N \times T) \times n \times C \qquad \text{(mGy cm)} \qquad (5)$$

where i is the number of scan sequences in the examination, each with n rotations of nominal beam collimation NxT (Equation 1, **but** expressed in cm) and radiographic exposure C mAs per rotation; ${}_nCTDI_w$ is the normalised weighted CTDI (mGy $mA^{-1}s^{-1}$) appropriate for the applied potential and total nominal beam collimation.

Alternatively, the DLP for each scan sequence is given by (McNitt-Gray, 2002):

$$DLP = CTDI_{vol} \times L \qquad \text{(mGy cm)} \qquad (6)$$

where L is the scan length (cm), limited by the outer margins of the exposed scan range, irrespective of pitch (which is, of course, already included in $CTDI_{vol}$). For a helical scan sequence, this is the total scan length that is exposed during (raw) data acquisition, including any additional rotation(s) at either end of the programmed scan length necessary for data interpolation (Nicholson and Fetherston, 2002). For serial scanning, L is the distance between the outer margins of the first and last slices in a sequence.

The DLP provides a broad indication of the energy imparted during a CT examination. Monitoring of DLP for a complete examination takes account of the volume of irradiation, as determined, for example, by the number of slices in serial scanning or the acquisition time in spiral scanning, and the number of such scan sequences conducted during the examination.

2.3.4 Relationship between effective dose and DLP

Values of such reference dose quantities provide useful indications of relative patient exposure for a given type of procedure. Values of DLP may also be used to derive broad estimates of effective dose (E) for CT procedures using region-specific coefficients. Initial values of E per DLP for CT examinations on adult patients were given by Shrimpton et al (1998) and Jessen et al (1999) based on early CTDI data, with final coefficients from more complete analyses being published by the European Commission (1999). Some preliminary values of E per DLP for paediatric CT have also been published (Shrimpton and Wall, 2000).

Values of E per DLP have also been derived from measurements with TLDs in a family of physical anthropomorphic phantoms representing ages 0 to 15 years (Chapple et al, 2002).

3 NEW MONTE CARLO CALCULATIONS FOR CT AT NRPB

Whereas in recent years CT has been a general focus for efforts in patient protection, optimisation of protection for paediatric CT is only now beginning to

achieve due prominence, following an earlier general lack of awareness of the potentially higher levels of dose (and risk) to children relative to adults (Rogers, 2001; Linton and Mettler, 2003; Wall, 2003). This unfortunate oversight was fostered, perhaps, by the absence of specific tools for paediatric CT dosimetry.

In order to facilitate more comprehensive dose assessment for CT, particularly in relation to examinations on children, new Monte Carlo simulations have been performed at NRPB for a complete family of six (MIRD) geometric mathematical phantoms representing ages from newborn to adult (Khursheed et al, 2002; this publication is reproduced in Appendix A). Organ doses have been calculated for CT exposures of contiguous, 1 cm thick, transverse slices in each phantom, and for three CT scanner models included in earlier work (Jones and Shrimpton, 1993): Siemens DRH, GE 9800 and Philips LX. This particular selection not only allowed benchmarking of results with data published previously for the adult, but it also covered a broad range of differences in CT scanner design (beam geometry and radiation quality, including the use of shaped filters). All calculations were implemented using the MCNP-4C radiation transport code operating on a personal computer (with Pentium III processor).

Rigorous quality assurance procedures were undertaken so as to validate the models developed (Khursheed et al, 2002; Appendix A). In particular, remarkably good agreement was found with the results of comparable Monte Carlo calculations previously completed at NRPB, in relation to both CT (of adults) (Jones and Shrimpton, 1993) and conventional x-ray exposures (Hart et al, 1994; Hart et al, 1996). In addition, calculations were also carried out in relation to values of CTDI at the centre ($CTDI_{100,c}$) and periphery ($CTDI_{100,p}$) of the standard head and body CT dosimetry phantoms. Calculated ratios of $CTDI_{100,p}$ to $CTDI_{100,c}$, and $CTDI_w$ to air kerma, were reassuringly close to measured values (ImPACT, 2002) for each of the three scanner models, as summarised in Table 1.

TABLE 1 Values of CTDI in standard CT dosimetry phantoms calculated by NRPB relative to measurements by ImPACT (2002)

Dosimetry phantom	Dose ratio	Relative to ImPACT measurements		
		Siemens DRH	GE 9800	Philips LX
Head	$CTDI_{100,p}$ / $CTDI_{100,c}$	1.00	0.92	1.02
	$CTDI_w$ / $CTDI_{air}$	0.97	1.06	1.06
Body	$CTDI_{100,p}$ / $CTDI_{100,c}$	1.00	0.91	1.08
	$CTDI_w$ / $CTDI_{air}$	0.99	1.02	1.15

In general, the organ dose calculations demonstrate that values of effective dose from CT, when normalised to air kerma, are significantly greater for paediatric patients than for adult patients when using the same technique to scan similar anatomical regions, but with some dependence on the scanner model. Both of these trends are demonstrated in Figures 1-4, which show the absolute values of normalised effective dose for scans over 4 regions of the body.

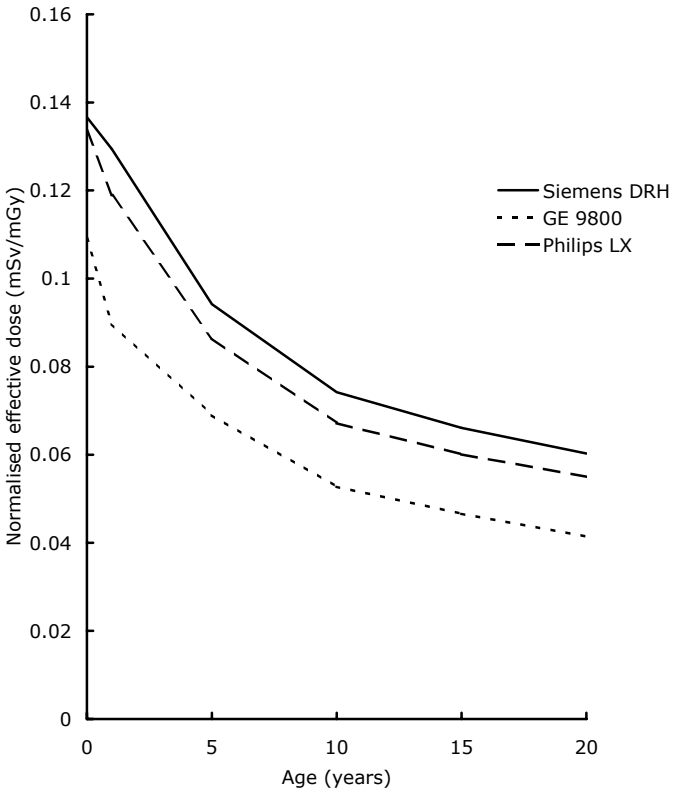

FIGURE 1 Effective dose normalised to $CTDI_{air}$ for examinations of the head & neck

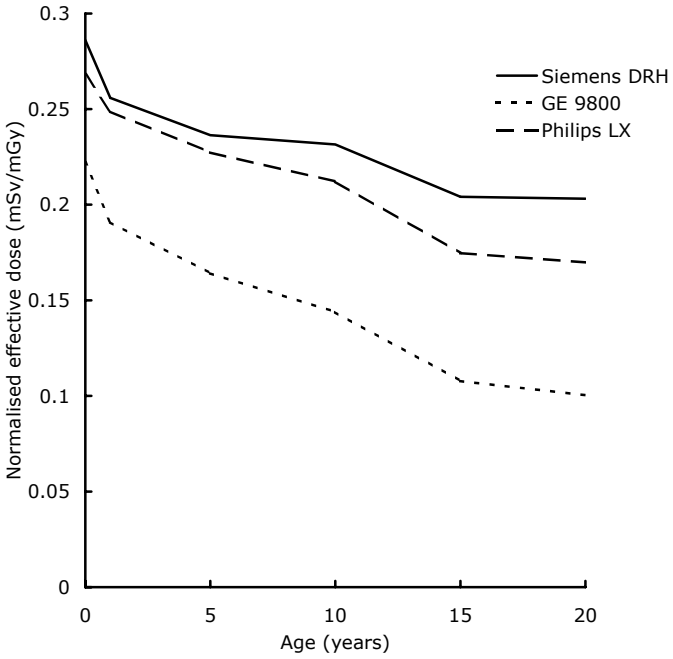

FIGURE 2 Effective dose normalised to $CTDI_{air}$ for examinations of the chest

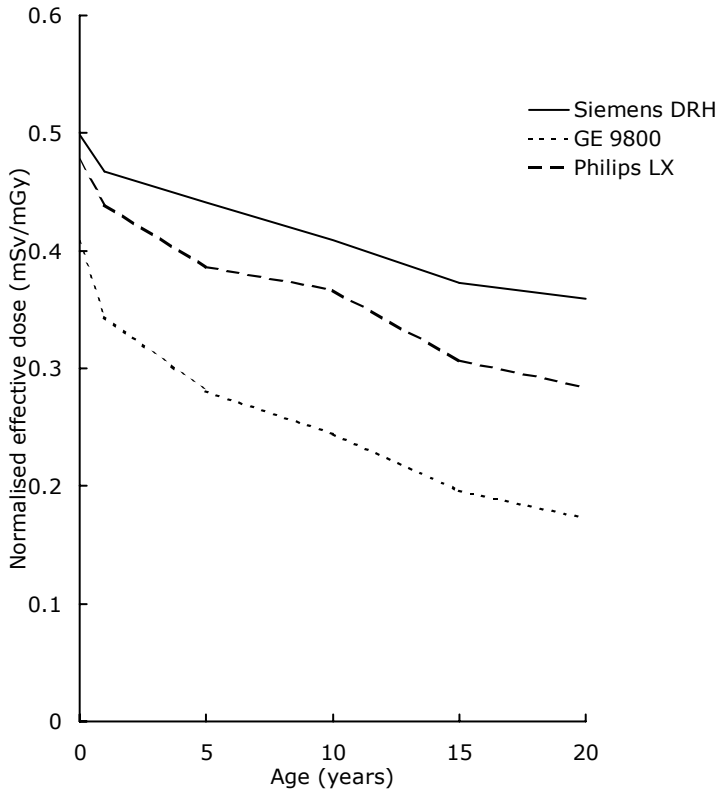

FIGURE 3 Effective dose normalised to $CTDI_{air}$ for examinations of the abdomen & pelvis

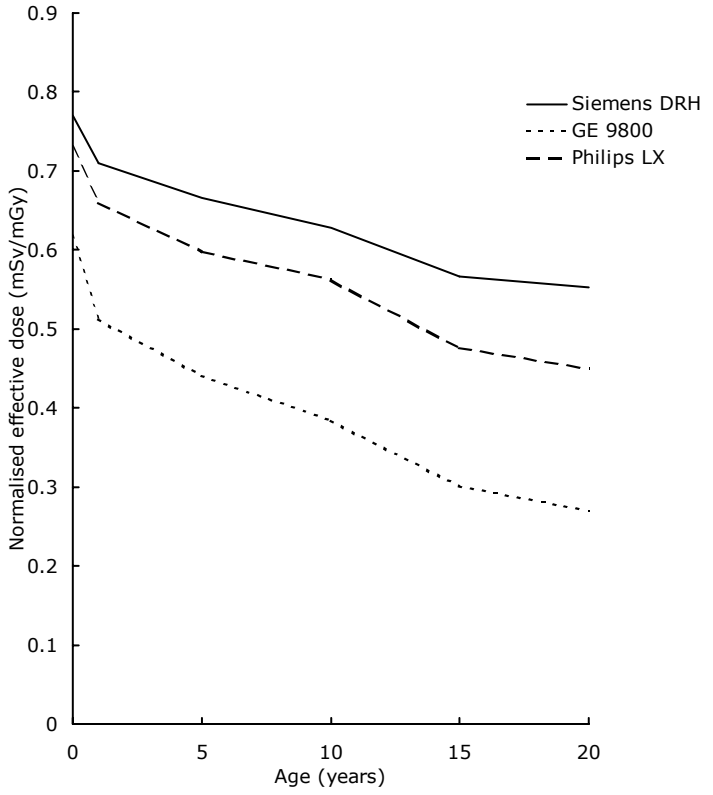

FIGURE 4 Effective dose normalised to $CTDI_{air}$ for examinations of the trunk

The relative increases in normalised dose for paediatric patients are illustrated more clearly in Figures A3-6 of Appendix A, where the dose data are shown relative to those for the adult. Differences in trends with age between scanner models are small for scans of the head and neck region (Figure A3), but more pronounced for scans of the chest (Figure A4), abdomen and pelvis (Figure A5) and trunk (Figure A6) regions. The enhancement in dose with decreasing phantom age is greatest for 'head and neck' scans, where it is in the range 2.3-2.6 for the newborn across all three scanners. For scans of the whole trunk, it ranges from 1.4 for the scanner without a shaped filter, the Siemens DRH, to 2.3 for the GE 9800 scanner. These trends are summarised in Table 2 in terms of general paediatric enhancement factors (PEFs) and discussed more fully in Appendix A.

TABLE 2 Relative trends in normalised effective dose for CT examinations on children

Age	Paediatric enhancement factor (PEF)	
	Head and neck region	Trunk region
Adult	1.0	1.0
15 y	1.1	1.0 – 1.1
10 y	1.2 – 1.3	1.1 – 1.4
5 y	1.6 – 1.7	1.2 – 1.6
1 y	2.2	1.3 – 1.9
0 y	2.3 – 2.6	1.4 – 2.3

Such paediatric enhancement factors provide a quick and simple way of broadly estimating effective doses to paediatric patients using the existing dose coefficients for adults; accordingly, PEFs have been incorporated into the ImPACT CT Dosimetry spreadsheet (ImPACT, 2003).

The results of these latest Monte Carlo calculations for CT are also summarised on the NRPB website:

http://www.nrpb.org/radiation_topics/medical/diagnostic_radiology/monte_carlo_calculations_patient_doses.htm.

4 NEW UNIVERSAL FRAMEWORK FOR CT DOSIMETRY

4.1 Universal organ dose coefficients

Organ dose coefficients for assessing patient doses in CT have thus far been normalised to the dose free-in-air on the axis of rotation of the scanner measured in the absence of the patient. Unfortunately, this approach provides coefficients that are significantly dependent upon the specific design of the scanner, with, for example, there being variations by up to a factor of three

between the different data sets for a range of 27 scanner models (Shrimpton and Edyvean, 1998). Accordingly, each new scanner model requires further Monte Carlo calculations to provide specific dose coefficients or some approximate matching to an existing data set (ImPACT, 2003), both of which are rather unsatisfactory steps.

A more elegant framework is likely to be provided if the calculated organ doses for the scanner are normalised to the corresponding values of weighted CTDI ($CTDI_w$) calculated for the standard (adult) head and body CT dosimetry phantoms. Since $CTDI_w$ takes due account of the impact of scanner design (particularly the shape of any bow-tie filter) on the dose distribution in the phantom, then using this quantity for normalisation should provide organ dose coefficients that are less scanner-specific than those based on $CTDI_{air}$. Such an approach holds the prospect of developing universal data sets that could subsequently be applied to assess patient doses for any model of scanner within acceptable uncertainties. Accordingly, analyses of the data from the new Monte Carlo calculations for CT at NRPB (Khursheed et al, 2002), when normalised to $CTDI_w$, are presented in Figures 5 to 8 in terms of normalised effective dose over 4 body regions for the three scanner models and 6 ages of phantoms. Normalisation is relative to $CTDI_w$ in the standard 16 cm diameter CT dosimetry phantom for all data except for the examinations on the body of the adult and the 15y old phantom, for which the 32 cm diameter CT dosimetry phantom has been used; hence the discontinuity and abrupt increase in normalised effective dose between ages 10y and 15y in Figures 6-8.

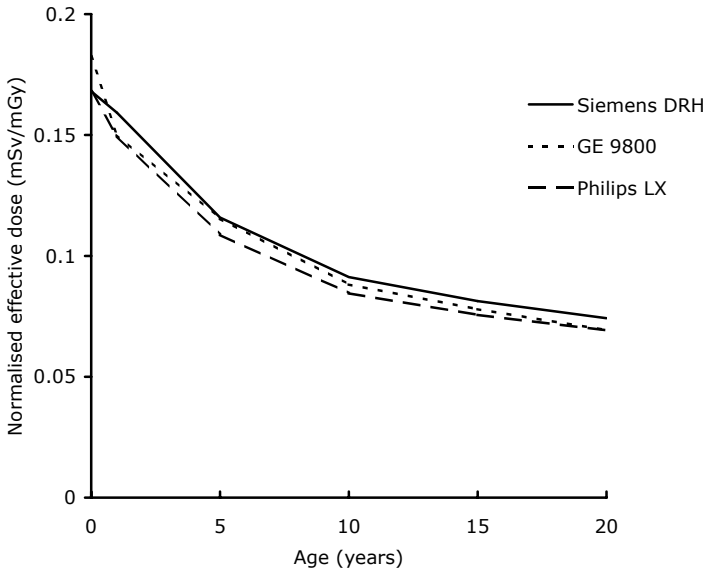

FIGURE 5 Effective dose normalised to $CTDI_w$ for examinations of the head & neck

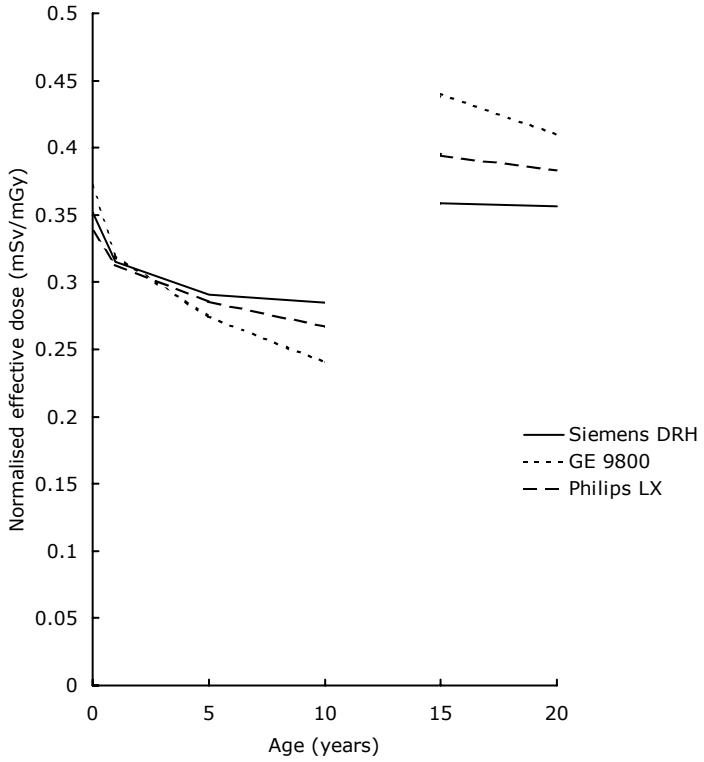

FIGURE 6 Effective dose normalised to $CTDI_w$ for examinations of the chest

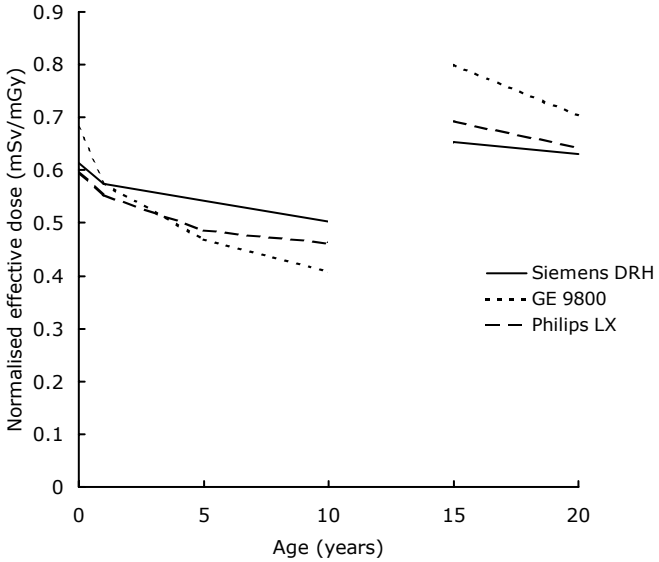

FIGURE 7 Effective dose normalised to $CTDI_w$ for examinations of the abdomen & pelvis

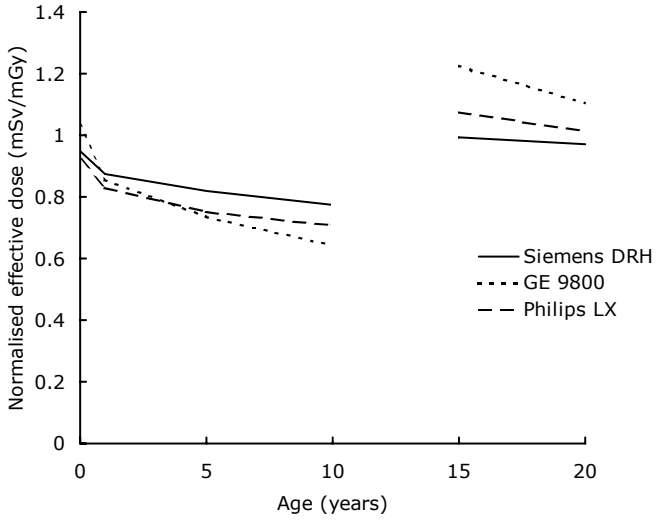

FIGURE 8 Effective dose normalised to $CTDI_w$ for examinations of the trunk

Normalisation to the weighted CTDI results in dose coefficients that are less dependent on scanner model, compared with normalisation to $CTDI_{air}$ (Figures 1-4), at least for the 3 particular models presently considered.

These normalised values of effective dose (relative to $CTDI_w$) are summarised in Table 3 by scanner model for each age and examination type, together with corresponding mean data and the integration lengths assumed for each scan. As a simplification, data for the 15y old phantom have been omitted since differences in physique and results between the adult and 15y old phantoms are relatively small; in any case, children of this age would in practice most likely be scanned using similar settings to those for adult patients. Coefficients of variation on the mean value of normalised effective dose for each phantom age and examination type lie in the range 1% to 10%. Furthermore, coefficients of variation for the normalised doses to individual organs range up to about 20% over the 3 data sets for significantly irradiated organs.

With such limited variation between the coefficients for the 3 scanner models of quite different design, mean data sets derived on a slab-by-slab basis for each of the 5 phantoms (with ages 0y, 1y, 5y, 10y and 20y (adult)) can be assumed to represent universal dose coefficients for application to any CT scanner. Clearly, the present analysis is based on rather limited data and ideally further calculations are required for a range of more modern scanners (including multi-slice systems) in order to validate the approach and provide more robust universal data sets. Nevertheless, the results of the present work appear encouraging in demonstrating the elements of a much simpler and universal framework for assessing doses for any scanner and patient age with reasonable uncertainties that are at least as good as those inherent in the present dosimetry methods involving scanner matching (ImPACT, 2003).

TABLE 3 Values of effective dose normalised to weighted CTDI

Examination	Age of phantom	Length of scan (cm)	Effective dose normalised to $CTDI_w$ (mSv mGy^{-1}) by scanner model				
			Siemens DRH	GE 9800	Philips LX	Mean value (& %CV)	
Head & neck[a]	0y	13	0.168	0.183	0.168	0.173	(4.8)
	1y	18	0.159	0.150	0.150	0.153	(3.5)
	5y	20	0.116	0.115	0.109	0.113	(3.5)
	10y	21	0.0913	0.0882	0.0845	0.0880	(3.8)
	Adult	23	0.0740	0.0691	0.0690	0.0707	(4.1)
Head[a]	0y	8	0.0876	0.0917	0.0853	0.0882	(3.7)
	1y	11	0.0784	0.0703	0.0718	0.0735	(5.9)
	5y	13	0.0569	0.0501	0.0508	0.0526	(7.1)
	10y	13	0.0444	0.0399	0.0407	0.0417	(5.8)
	Adult	13	0.0296	0.0265	0.0274	0.0278	(5.6)
Neck[a]	0y	5	0.0827	0.0933	0.0849	0.0869	(6.4)
	1y	7	0.0826	0.0816	0.0796	0.0812	(1.9)
	5y	7	0.0754	0.0815	0.0737	0.0769	(5.3)
	10y	8	0.0641	0.0651	0.0604	0.0632	(3.9)
	Adult	10	0.0612	0.0585	0.0576	0.0591	(3.1)
Chest[b]	0y	9	0.352	0.372	0.337	0.354	(4.9)
	1y	12	0.315	0.319	0.313	0.316	(1.0)
	5y	16	0.291	0.274	0.286	0.284	(3.0)
	10y	20	0.285	0.241	0.267	0.264	(8.4)
	Adult	27	0.357	0.410	0.383	0.383	(6.9)
Abdomen & pelvis[b]	0y	13	0.613	0.683	0.599	0.632	(7.1)
	1y	19	0.575	0.576	0.553	0.568	(2.3)
	5y	25	0.542	0.470	0.486	0.499	(7.6)
	10y	31	0.503	0.408	0.462	0.458	(10)
	Adult	43	0.631	0.704	0.642	0.659	(6.0)
Trunk[b]	0y	22	0.948	1.03	0.919	0.967	(6.2)
	1y	31	0.873	0.856	0.830	0.853	(2.5)
	5y	41	0.819	0.737	0.751	0.769	(5.7)
	10y	51	0.774	0.642	0.708	0.708	(9.3)
	Adult	70	0.970	1.10	1.01	1.03	(6.5)

[a]All data normalised to $CTDI_w$ in the standard head CT dosimetry phantom.

[b]Data for adult normalised to $CTDI_w$ in the standard body CT dosimetry phantom; data for all other ages of mathematical phantom normalised to $CTDI_w$ in the standard head CT dosimetry phantom.

4.2 Estimating effective dose from DLP

On the basis of the above analysis, some initial coefficients have been derived relating effective dose (E) and dose-length product (DLP) for the various standard body regions and mathematical phantoms. These data are shown in

Table 4 and represent mean values for the three scanner models studied; coefficients of variation and assumed scan lengths are as given in Table 3.

The coefficients for effective dose vary with anatomical region, reflecting the relative distribution of radiosensitive organs within the body (Shrimpton et al, 1991). However, the data in Table 4 provide a practical way of estimating effective dose when the region of scan is similar to that assumed when deriving the average coefficient, with there being some residual sensitivity to the relative location or length for a particular scan.

TABLE 4 Normalised values of effective dose per dose-length product (DLP) over various body regions and (standard) patient age

Region of body	Effective dose per DLP (mSv (mGy cm)$^{-1}$) by age				
	0[a]	1y[a]	5y[a]	10y[a]	Adult[b]
Head & neck	0.013	0.0085	0.0057	0.0042	0.0031
Head	0.011	0.0067	0.0040	0.0032	0.0021
Neck	0.017	0.012	0.011	0.0079	0.0059
Chest	0.039	0.026	0.018	0.013	0.014
Abdomen & pelvis	0.049	0.030	0.020	0.015	0.015
Trunk	0.044	0.028	0.019	0.014	0.015

[a]All data normalised to $CTDI_w$ in the standard head CT dosimetry phantom.

[b]Data for the head & neck regions normalised to $CTDI_w$ in the standard head CT dosimetry phantom; data for other regions normalised to $CTDI_w$ in the standard body CT dosimetry phantom.

When due account is taken of differences in integration length and in the methods used to calculate organ and effective doses for similar coefficients from earlier studies, the present data are broadly consistent with previous coefficients published for adult patients (European Commission, 1999). However, the trends for relative increases in dose to small patients (for constant exposure settings) are less pronounced than those previously derived on the general basis of energy imparted rather than organ doses (Shrimpton and Wall, 2000). Further detailed analyses and comparisons are in progress.

5 CONCLUSIONS

The increasing application of CT in clinical practice ensures the continuing need for practical dosimetry as an essential element of patient protection. Review of this important topic has concluded that the existing framework for reference doses can easily be adapted to include subsequent developments in technology, such as multislice CT and the requirement for display of volume CTDI. However, limitations are also apparent in the present methods for assessing organ and effective doses when applied to new scanner models and paediatric patients. Accordingly, new series of Monte Carlo calculations have been carried out at NRPB for a family of 6 geometric mathematical phantoms representing ages

from newborn to adult. These have formed the basis for the derivation of broad paediatric enhancement factors, which summarise the increased doses to small children relative to those to adults under similar conditions of CT exposure. Furthermore, analyses of results from the calculations suggest that normalisation of organ doses to values of weighted CTDI (rather than axial air kerma) could provide a more elegant and simpler framework for the universal assessment of doses to all ages of patient and all scanner models. Further calculations and data analysis are required in order to build confidence in the proposed framework and to provide more definitive dose coefficients, applicable to the latest developments in CT technology.

6 REFERENCES

Alonso M, Barriuso T, Castañeda MJ, Díaz-Caneja N, Gutiérrez I and Villar E (2002). Monte Carlo estimation of absorbed dose to organs in computed tomography. *Health Physics*, **82**, No 2, 233-239.

Atherton JV and Huda W (1996). Energy imparted and effective doses in computed tomgraphy. *Med Phys*, **23**, No 5, 735-741.

Baadegaard N and Jensen LC (1999). CT Dose v 0.67. Herlev Denmark, National Institute of Radiation Hygiene.

Chapple C-L, Willis S and Frame J (2002). Effective dose in paediatric computed tomography. *Phys Med Biol*, **47**, 107-115.

European Commission (1997). European Commission Council Directive 97/43/EURATOM of 30 June 1997 on health protection of individuals against the dangers of ionising radiation in relation to medical exposure. *Off J Eur Commun*, **L180**, 22-27.

European Commission (1999). European guidelines on quality criteria for computed tomography. EUR 16262 EN. Luxembourg, Office for Official Publications of the European Communities.

Golding SJ and Shrimpton PC (2002). Radiation dose in CT: are we meeting the challenge. *Br J Radiol*, **75**, 1-4.

Hart D, Jones DG and Wall BF (1994). Normalised organ doses for medical x-ray examinations calculated using Monte Carlo techniques. Chilton, NRPB-SR262.

Hart D, Jones DG and Wall BF (1996). Normalised organ doses for paediatric x-ray examinations calculated using Monte Carlo techniques. Chilton, NRPB-SR279.

Huda W and Atherton JV (1995). Energy imparted in computed tomgraphy. *Med Phys*, **22**, No 8, 1263-1269.

Huda W, Atherton JV, Ware DE and Cumming WA (1997). An approach for the estimation of effective radiation dose at CT in pediatric patients. *Radiology*, **203**, 417-422.

Huda W, Scalzetti EM and Roskopf M (2000). Effective doses to patients undergoing thoracic computed tomography examinations. *Med Phys*, **27**, No 5, 838-844.

Huda W, Scalzetti EM and Levin G (2001). Technique factors and image quality as functions of patient weight at abdominal CT. *Radiology*, **217**, 430-445.

Huda W, Chamberlain CC, Rosenbaum AE and Garrisi W (2001). Radiation doses to infants and adults undergoing head CT examinations. *Med Phys*, **28**, No 3, 393-399.

IAEA (1996). International basic safety standards for protection against ionizing radiation and for the safety of radiation sources. IAEA Safety Series 115. Vienna, International Atomic Energy Agency.

ICRP (1996). Radiological protection and safety in medicine. International Commission on Radiological Protection Publication 73. *Annals of the ICRP*, **26** No 2. Oxford, Pergamon.

ICRP (2000). Managing patient dose in computed tomography. International Commission on Radiological Protection Publication 87. *Annals of the ICRP*, **30**, No 4. Oxford, Pergamon.

IEC (2003). Medical Electrical Equipment – Part 2-44: Particular requirements for the safety of x-ray equipment for computed tomography. International Electroctechnical Commission Standard 60601-2-44 Ed 2 Amendment 1. Geneva, IEC.

ImPACT (2002). CT patient dosimetry Excel spreadsheet v0.99m (1/7/02). Available from home webpage of the ImPACT (Imaging Performance and Assessment of CT scanners) evaluation centre of the DH Medical Devices Agency, http://www.impactscan.org.

ImPACT (2003). CT patient dosimetry Excel spreadsheet v0.99u (12/12/03). Available from home webpage of the ImPACT (Imaging Performance and Assessment of CT scanners) evaluation centre of the DH Medical Devices Agency, http://www.impactscan.org.

IPEM (2003). Measurement of the performance characteristics of diagnostic x-ray systems used in medicine. IPEM Report No 32 Part III: Computed tomography x-ray scanners (2nd edition). York, Institute of Physics and Engineering in Medicine.

IRMER (2000). The Ionising Radiation (Medical Exposure) Regulations 2000. SI (2000) No. 1059. TSO, London.

Jansen JThM, Geleijns J, Zweers D, Schultz FW and Zoetelief J (1996). Calculation of computed tomography dose index to effective dose conversion factors based on measurement of the dose profile along the fan shaped beam. *Br J Radiol*, **69**, 33-41.

Jarry G, DeMarco JJ, Beifuss U, Cagnon CH and McNitt-Gray MF (2003). A Monte Carlo-based method to estimate radiation dose from spiral CT: from phantom testing to patient-specific models. *Phys Med Biol*, **48**, 2645-2663.

Jessen KA, Shrimpton PC, Geleijns J, Panzer W and Tosi G (1999). Dosimetry for optimisation of patient protection in computed tomography. *Appl Radiat Isot*, **50**, No 1, 165-172.

Jones DG and Shrimpton PC (1991). Survey of CT practice in the UK. Part 3: Normalised organ doses calculated using Monte Carlo techniques. Chilton, NRPB-R250.

Jones DG and Shrimpton PC (1993). Normalised organ doses for x-ray computed tomography calculated using Monte Carlo techniques. Chilton, NRPB-SR250.

Kalender WA, Schmidt B, Zankl M and Schmidt M (1999). A PC program for estimating organ and effective dose values in computed tomography. *Eur Radiol*, **9**, 555-562.

Khursheed A, Hillier MC, Shrimpton PC and Wall BF (2002). Influence of patient age on normalized effective doses calculated for CT examinations. *Br J Radiol*, **75**, 819-830.

Le Heron JC (1993). CTDOSE. Christchurch NZ, National Radiation Laboratory.

Leitz W, Axelsson B and Szendrö G (1995). Computed tomography dose assessment – a practical approach. *Radiat Prot Dosim*, **57**, Nos 1-4, 377-380.

Linton OW and Mettler FA (2003). National conference on dose reduction in CT, with an emphasis on pediatric patients. *AJR*, **181**, 321-329.

McCollough CH (2000). Calculation of effective dose. *Med Phys*, **27**, No 5, 828-837.

McNitt-Gray MF (2002). Radiation dose in CT. *Radiographics*, **22**, 1541-1553.

Nagel HD (ed.) (2002). Radiation exposure in computed tomography (4th edition). Hamburg, CTB Publications.

Nicholson R and Fetherston S (2002). Primary radiation outside the imaged volume of a multislice helical CT scan. *Br J Radiol*, **75**, 518-522.

Petoussi-Hens N, Zankl M, Fill U and Regulla D (2002). The GSF family of voxel phantoms. *Phys Med Biol*, **47**, 89-106.

Rogers LF (2001). Taking care of children: check out the parameters used for helical CT. *AJR*, **176**, 287.

Schmidt B and Kalender WA (2002). A fast voxel-based Monte Carlo method for scanner- and patient-specific dose calculations in computed tomography. *Physica Medica*, **XVIII**, No 2, 43-53.

Shrimpton PC (1997). Reference doses for computed tomography. *Radiol Prot Bull*, No 193, 16-19.

Shrimpton PC (1999). At home in Aarhus. *Radiol Prot Bull*, No 214, 18-19.

Shrimpton PC (2002). The need for dose measurement and reference levels in diagnostic radiology. IN *Patient Dose Levels and Risk in Diagnostic Radiology.* Newcastle Medical Radiation Symposium 2000 (HM Warren-Forward, editor), pp3-11. Newcastle NSW, The University of Newcastle.

Shrimpton PC and Edyvean S (1998). CT scanner dosimetry. *Br J Radiol*, **71**, 1-3.

Shrimpton PC, Jessen KA, Geleijns J, Panzer W and Tosi G (1998). Reference doses in computed tomography. *Radiat Prot Dosim*, **80**, Nos 1-3, 55-59.

Shrimpton PC, Jones DG, Hiller MC, Wall BF, Le Heron, JC and Faulkner K (1991). Survey of CT practice in the UK. Part 2: Dosimetric aspects. Chilton, NRPB-R249.

Shrimpton PC and Wall BF (2000). Reference doses for paediatric computed tomography. *Radiat Prot Dosim*, **90**, Nos 1-2, 249-252.

UNSCEAR (2000). Sources and effects of ionizing radiation. United Nations Scientific Committee on the Effects of Atomic Radiation 2000 Report to the General Assembly, with Scientific Annexes. Volume I: Sources. UN Sales Publication E.00.IX.3. New York, United Nations.

Wall BF (2003). What needs to be done about reducing patient doses from CT? The North American approach. *Br J Radiol*, **76**, 763-765.

Wall BF and Shrimpton PC (1998). The historical development of reference doses in diagnostic radiology. *Radiat Prot Dosim*, **80**, Nos 1-3, 15-20.

Wise KN (1994). An EGS4 based mathematical phantom for radiation protection calculations using standard man. *Health Physics*, **67**, No 5, 548-553.

Zankl M, Panzer W and Drexler G (1991). The calculation of dose from external photon exposures using reference human phantoms and Monte Carlo methods. Part VI: Organ doses from computed tomographic examinations. GSF-Bericht 30/91. Neuherberg, Gesellschaft für Strahlen- und Umweltforschung.

APPENDIX A

INFLUENCE OF PATIENT AGE ON NORMALIZED EFFECTIVE DOSES CALCULATED FOR CT EXAMINATIONS*

A KHURSHEED, PHD, MC HILLIER, PC SHRIMPTON, PHD AND BF WALL, BSC

NATIONAL RADIOLOGICAL PROTECTION BOARD, CHILTON, DIDCOT, OXFORDSHIRE OX11 0RQ, UK

Abstract Monte Carlo simulations of CT examinations have been performed to estimate effective doses, normalized to axial air kerma, for six mathematical phantoms representing ages from newborn to adult, and for three CT scanner models covering a range of designs. Organ doses were calculated for CT exposures of contiguous, 1 cm wide, transverse slices in each phantom and summed to give normalized effective doses for scans of four regions of the trunk and head. In all cases an inverse trend is observed between normalized effective dose and phantom age, with the dose to the newborn from head and neck scans being 2.2–2.5 times higher than that to the adult, depending on scanner model. Corresponding increases for scans of the trunk region are more variable between scanners and range from a factor of 1.3 to 2.4. If typical clinical exposure conditions for adults are also utilized for children, then, for example, the effective dose to the newborn from a chest scan could be above 15 mSv. It is concluded that CT has the potential to deliver significantly greater radiation doses to children than to adults and in view of their greater susceptibility to radiation effects, special efforts should be made in clinical practice to reduce doses to children by the use of size-specific scan protocols.

CT provides high quality X-ray imaging with substantial benefits in healthcare, although patient doses are relatively high, often exceeding 10 mSv effective dose per examination. Clinical application of the technique has continued to increase such that CT examinations now account for approximately 40% of the annual collective dose from medical X-rays in the UK whilst representing only 5% of their total number [A1], much in line with practice in other developed countries [A2]. Significant numbers of CT procedures are conducted on young patients; studies on children aged 0–15 years comprised, for example, 11% of all CT procedures at one large US hospital [A3] and 6% on average in some other developed countries [A2]. Lifetime radiation risks per unit effective dose

* First published in the British Journal of Radiology, 75 (2002), 819-830

are likely to be higher for those exposed in childhood rather than later life [A4]. This probable enhancement of risk, together with evidence for the inconsistent use of specific scan protocols tailored to small patients, ensures that paediatric CT remains a focus for initiatives in radiation protection [A5, A6].

Dosimetry is an essential element of patient protection. Monte Carlo calculations in particular have already provided coefficients that facilitate the estimation of organ doses for CT scans on adult patients [A7–9]. However, similar data for paediatric CT have so far been available in relation to a few voxel phantoms derived from specific patients; a baby aged 8 weeks and a child aged 7 years [A10], and a 14 year-old girl [A11]. Some organ dose measurements have also been reported for standard examinations and specific paediatric physical phantoms [A12, A13]. More generally, Huda et al [A14] have predicted significant increases in effective dose for examinations of the head and abdomen with decreasing patient size and constant exposure (mAs) setting, although these trends are derived on the broad basis of energy imparted rather than organ doses.

The existing dose coefficients for CT published by the National Radiological Protection Board (NRPB) [A9] have now been supplemented by further calculations for a complete family of six geometric phantoms, representing patients of age newborn, 1 year, 5 years, 10 years, 15 years and adult, based on those of Cristy and Eckerman [A15]. Calculations have been performed for three sets of CT exposure conditions modelled in the earlier work, corresponding to the Siemens DRH (Siemens Medical Systems, Forcheim, Germany), GE 9800 (General Electric Medical Systems, Milwaukee, WI) and Philips LX (Philips Medical Systems, Best, The Netherlands) scanners. This particular selection not only allows benchmarking of results with published data for the adult, but it also covers a broad range of differences in CT scanner design (beam geometry and radiation quality). Values of effective dose normalized to absorbed dose free-in-air on the axis of rotation for examinations of adults for these three scanners are widely spaced in the range of such data observed in calculations for 27 models of CT scanner [A16].

Detailed results from the present calculations will be available in due course as a software report providing normalized organ doses for the irradiation of each 1 cm transverse slice of each phantom. This paper presents a broad summary of the computational methods used and an initial analysis of the trends, illustrating the likely increases in effective doses to children from CT without changes in technique to account for patient size.

A1 Method

A1.1 Monte Carlo methods

The application of Monte Carlo methods for simulating radiation transport and energy deposition in anthropomorphic phantoms is well established. The underlying principle for such methods is the assignment of probability functions

to the physical interactions that may occur as a particle travels through a medium. A physics ''history'' of a fictitious individual particle is constructed by applying random number inputs to the probability functions for these particle interactions. By generating a statistically large number of particle histories, it is possible to predict such properties of a radiation field as the particle fluence, energy deposition and energy spectrum at particular points. The accuracy of the method increases proportionally with the number of particle histories in a manner that is described by Poisson statistics.

Here the method is used to predict energy deposition in the tissues of an anthropomorphic phantom from a rotating X-ray source. It was found that more than 100 000 particle histories are required to produce a statistically meaningful result for major organs lying within the beam of a single CT slice of 1 cm width. Advances in the power of personal computers mean that Monte Carlo simulations may now be run on the new generation of relatively inexpensive personal computers. A calculation with 250 000 histories takes approximately 5 min to execute on the Pentium III processor (Intel Corporation, Santa Clara, CA) used for these simulations.

The Monte Carlo N-Particle (MCNP) radiation transport code [A17] was used in this work. Originally developed for the study of neutrons at Los Alamos for the Manhattan Project, the code has been adapted for a wider range of particles and is currently one of the most widely used general purpose Monte Carlo codes in the world. In particular, it contains a combinatorial description of geometry, which makes it suited to the geometric surfaces used in mathematical phantoms. At present, the main drawback of the code for medical applications would appear to be that it is slower to execute than other codes, such as EGS4 [A18], owing to its large number of input options. Since approximately 2000 simulations were performed in this study for three CT scanners, this is obviously an important issue.

A1.2 Phantom implementation

Some changes were made to the Cristy and Eckerman [A15] phantoms. The thyroid gland described by Cristy and Eckerman was changed since it contained surface equations that were higher than second order, which could not be accommodated by MCNP. A thyroid composed of two cylindrical lobes with the same mass and centroid as the original was used instead. A chin was added so that the thyroid gland would be embedded at a realistic distance from the surface of the neck. The detailed heart model was simplified into muscle surrounding a volume of blood; this was because the heart does not figure explicitly in the calculation of effective dose. An oesophagus, based upon that in the adult phantom of Zankl et al [A19], was added in order to calculate effective dose. It was scaled according to mass for paediatric phantoms. The trunk of the phantom was divided into six segments in order to simplify the shapes of the soft tissue cells that surround the organs. This was necessary since there is a limit to the number of surfaces that may be used to describe a cell in MCNP.

There are also differences between the adult phantom used here and that used in earlier NRPB CT dose calculations [A8, A9]. This earlier work did not specifically model the oesophagus and the dose to the thymus was used in its place for the calculation of effective dose. It also assumed that the breast was composed of a 50/50 mix of fat and soft tissue. Since it is known that the fat content of breast tissue is lower in young women, it seemed more appropriate that the composition of the breast in the paediatric phantoms used here is entirely soft tissue. For consistency and convenience the same composition was used for the adult phantom.

A1.3 X-ray source description for CT

CT scans were simulated by exposing a series of contiguous transverse slices of 1 cm thickness in each phantom to X-rays emitted from sources lying on a circle around the phantom in the same plane as each slice. The slices covered the entire length of the smaller phantoms and at least the regions commonly scanned from the top of the head to the knees in the larger phantoms. For each

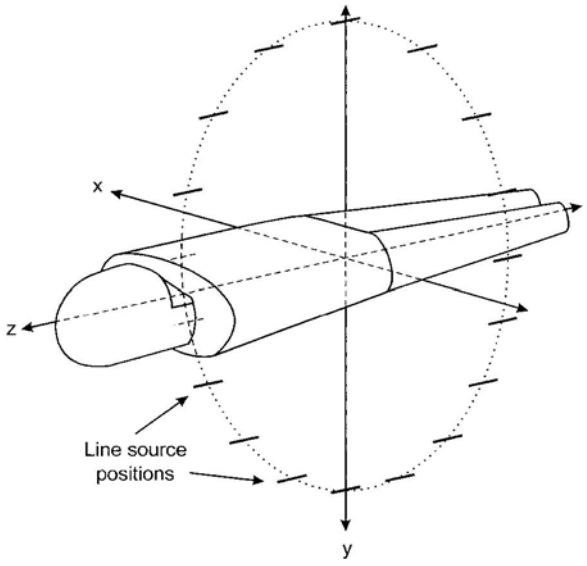

FIGURE A1 Representation of X-ray source for a CT slice.

slice position, the source position is randomly sampled from a number of 1 cm long line sources, parallel to the axis of rotation of the scanner, on a circle with radius equal to the focus-to-axis distance for the scanner in question (Figure A1). Photons are emitted normal to each line source, but unconstrained otherwise, i.e. over 360°. It follows that most source photons will not interact with the phantoms, but these photon histories add little to computational overheads since they are quickly ''killed'' when the photons reach a predetermined distance from the phantoms. The photons that are tracked through the phantoms essentially arise from a fan-shaped beam from each source that is perfectly collimated to the phantom and has parallel sides 1 cm apart.

In practice, the collimation of CT scanner beams in the z-direction (along the axis of rotation) is not perfect and the sides of the fan beam are slightly diverging. This divergence results in overlapping of contiguous scans and an increase in dose to the patient. The degree of divergence is scanner-specific and can be difficult to ascertain in practice. However, it can be taken into account by measuring the CT dose index (CTDI) [A20]. CTDI is essentially the integral of the absorbed dose in the z-direction divided by the nominal slice width. Since the Monte Carlo calculations model all the scattering that takes place inside the phantoms, it is the CTDI measured free-in-air on the axis of rotation that will provide the necessary measure of the effect of the actual beam divergence on organ doses. In this work, the calculated organ doses are normalized to the absorbed dose on the scanner axis free-in-air (with perfect collimation). Multiplying the normalized organ doses by the CTDI measured free-in-air on the axis of rotation for the particular scanner in question will provide organ doses that reflect the level of beam collimation achieved by that particular scanner.

Three scanner models were used, covering a range of design; a Siemens DRH, a GE 9800 and a Philips LX. In the Philips LX and GE 9800 scanners the X-ray beam passes through both flat and shaped filters, whereas in the Siemens DRH scanner there is only a flat filter. For the first two scanners, the shaped filters were modelled in the Monte Carlo calculations using shape and composition data from the manufacturers. The filters were situated radially inside each line source (Figure A2), and their lateral extent effectively limited to 18, the number of line sources that could be fitted around the circle describing the source geometry. For the Siemens DRH scanner, with just a simple flat filter, the number of sources that could be fitted into the circle was not limited by geometry constraints, and was chosen to be 72. A comparison was made between doses received by the adult phantom from implementations of the Siemens DRH scanner with both 18 and 72 line sources; differences between organ doses were small and within statistical uncertainties for each 1 cm slice (generally <5% for small organs and <2% for larger organs). It was thus shown that 18 sources were sufficient to approximate the continuous circular movement of the source, without significantly affecting the calculated organ doses.

The physical characteristics of the three scanners modelled in this study are summarized in Table A1. They were primarily chosen to cover the range of different scanner characteristics seen in an earlier study [A8], which led to significant differences in the normalized organ doses previously calculated for these three scanners. The choice was particularly influenced by the need to cover the wide range of filtration that exists for CT scanners. The flat filters in these three scanners ranged from 2.7 mm aluminium (Al) equivalent for the GE 9800, to 7.4 mm for the Siemens DRH. In addition, the GE 9800 and Philips LX have shaped filters made from polytetrafluoroethylene and Al, respectively. Note that for examinations of adults it is possible to match these scanner models to more current models, based on dosimetric characteristics, by following the procedure suggested by ImPACT [A21].

A1.4 Source energy spectra

Photon energy spectra at source, following passage through the flat filters, were generated for the three scanners from the Institute of Physics and Engineering in Medicine (IPEM) catalogue of X-ray spectra [A22]. Tube voltages, flat filtration and anode angles, given in Table A1, were those specified by the manufacturers. It was noted that the resulting energy spectra were sensitive to anode angle, a parameter that is known to vary significantly between different types of X-ray tube.

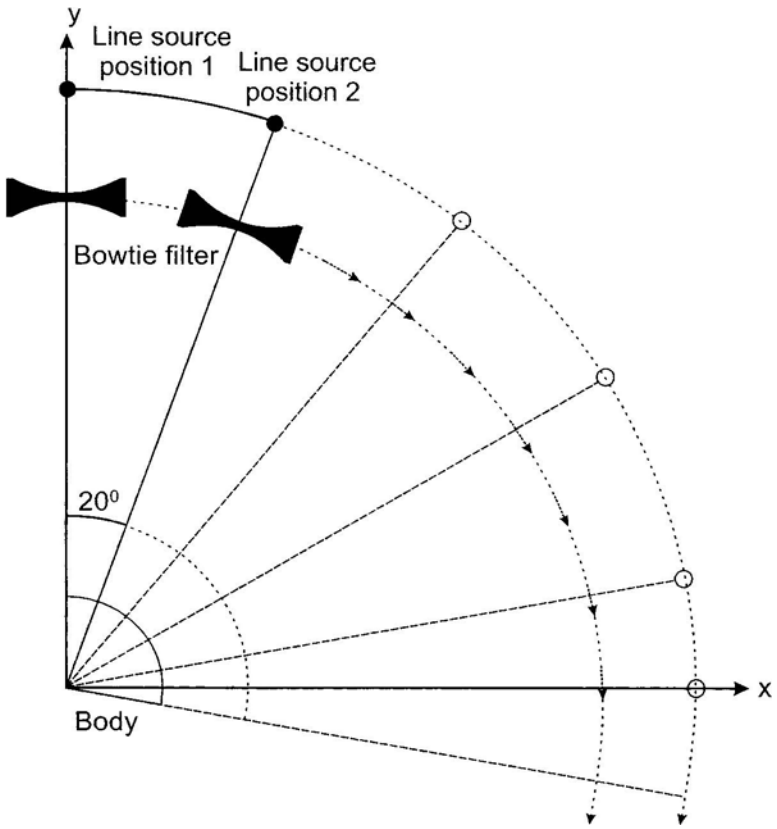

FIGURE A2 Positioning of bow tie filters relative to line sources.

It has been shown that organ doses are sensitive to the energy spectra used in the calculations [A11]. Spectra produced from the IPEM catalogue [A22] were therefore compared with those produced from an earlier catalogue [A23] for the same tube voltages, anode angles and flat filtration, but without filtration from shaped filters. The half-value layers (HVL) and mean energies of the two sets of spectra are very similar (see Table A1).

HVLs are also available for the three scanners, which include filtration through the thin central section of the shaped filters, when present. These have been measured by the ImPACT Group at St George's Hospital, London (S Edyvean, personal communication) and are shown in the last row of Table A1. For the Siemens DRH scanner, which does not contain a shaped filter, the measured HVL is in good agreement with the calculated HVL. Measured HVLs for the other two

scanners are significantly greater than calculated HVLs, indicating that the beam quality has been changed by passage through the centre of the shaped filters. Differences in the measured HVLs between scanners are narrow, with that for the GE 9800 being slightly less than for the other two scanners. However, it should be noted that, owing to the shaped filters, the HVLs of the GE and Philips scanner spectra will increase (and the photon fluence fall) off the scanner axis of rotation.

Table A1 Physical characteristics of scanners in the study

	Siemens DRH	Philips LX	GE 9800
Tube voltage (kVp)	125	120	120
Focus-to-axis distance (mm)	700	606	630
Flat filter (mm Al Equivalent)	7.4	4.5	2.7
Shaped filter material	None	Al	PTFE
Anode angle	12°	7°	6°
HVL (mm Al)[a] [A21]	8.02	6.77	5.75
Mean energy (keV) [A21]	64.6	60.9	58.7
HVL (mm Al)[a] [A22]	7.97	6.58	5.70
Mean energy (keV) [A22]	64.5	60.2	58.0
HVL (mm Al)[b] — measured	7.9	7.9	7.2

Al, aluminium; HVL, half-value layer.

[a]Before passage through shaped filter.

[b]After passage through shaped filter.

A1.5 Dosimetry

For each Monte Carlo simulation, energy deposition was tallied for 37 geometric regions, which correspond to whole organs, tissue compartments or bones in the anthropomorphic phantoms. Mean organ doses for CT scans of each 1 cm slice of the phantom were normalized to the absorbed dose to air (or the air kerma) on the axis of rotation in the absence of the phantom. Results are therefore independent of X-ray tube output, which is desirable since the selection of tube current and scan time are largely at the discretion of the user and the tube output per mAs may vary markedly between scanners of the same make and model. To convert these normalized doses into absolute organ doses it is necessary to multiply them by the CTDI measured free-in-air on the axis of rotation for the particular CT scanner model and exposure conditions required.

No attempt is made to model the complex distribution of bone marrow and endosteal bone surfaces in the skeleton of the phantoms. The model assumes a uniform mix of bone and marrow in all parts of the skeleton. Dose to bone marrow is enhanced by its proximity to bone, and was calculated in a similar manner to that of Jones and Wall [A24]. Bone marrow dose enhancement factors for each bone type, i, as described by Wall et al [A25] as a function of photon energy, were weighted by the energy spectrum of the Siemens scanner. The resulting energy-averaged enhancement factors, h_{mi}, are used to calculate

bone marrow dose from the energy deposited in the marrow-bone mixture in the following manner. For skeletal region *i* the energy deposited in the red bone marrow, E_{mi}, is related to the energy deposited in the marrowbone mixture, E_{si}, by

$$E_{mi} = E_{si}\, W_{mi}\, h_{mi}\, [(\mu_{en}/\rho)_m/(\mu_{en}/\rho)_s] \qquad \text{(A1)}$$

where W_{mi} is the fraction of total red bone marrow mass that is in region *i* and $(\mu_{en}/\rho)_m/(\mu_{en}/\rho)_s$ is the ratio of mass energy absorption coefficients for red bone marrow and for the marrow-bone mixture. Mean dose to the entire bone marrow, D_{rbm}, is then

$$D_{rbm} = \sum_i E_{mi}/M \qquad \text{(A2)}$$

where M is the total mass of red bone marrow in the phantom. Mass and distribution of bone marrow is taken from Cristy and Eckerman [A15]. The marrow dose enhancement factor is highest for the skull, for which it is 1.34 for the newborn and 1.21 for the adult, but is more typically in the range 1.10–1.15 for the rest of the skeleton.

A similar treatment was used to calculate doses to endosteal surfaces. In this case, however, a single energy-averaged endosteal surfaces dose enhancement factor, h_e, was calculated for the whole skeleton from data given by Wall et al [A25]. Energy deposited in endosteal surfaces in region *i* of the skeleton, E_{ei}, is thus given by

$$E_{ei} = E_{si}\, h_e\, [(\mu_{en}/\rho)_e/(\mu_{en}/\rho)_s] \qquad \text{(A3)}$$

where $[(\mu_{en}/\rho)_e/(\mu_{en}/\rho)_s$ is the ratio of mass energy absorption coefficients for endosteal surface tissues and the marrow-bone mixture. Owing to the different geometry that applies to endosteal surfaces, which are soft tissue layers (taken by the International Commission on Radiological Protection to be 10 microns thick) lying adjacent to the internal surfaces of hard bone, the enhancement factor is rather higher than for bone marrow. It ranges in value from 2.11 for the newborn to 1.85 for the adult. Mean dose to the whole endosteal surfaces, D_{es}, is then

$$D_{es} = \sum_i m_i\, E_{ei}\, /M_s \qquad \text{(A4)}$$

where m_i is the mass of skeleton region *i* and M_s is the total mass of the skeleton.

A1.6 Model validation

The family of anthropomorphic phantoms was implemented in the MCNP input file directly from the phantom descriptions furnished by Cristy and Eckerman [A15], together with the modifications discussed. Rigorous quality assurance procedures were essential to ensure correct implementation of the model, since each phantom plus the CT source description contain approximately 200

surfaces plus related transformations, and up to 150 input files were created for each phantom (one for each slice). The following five steps were taken:

(i) Organ volumes in the implemented phantoms were calculated by a ray-tracing procedure [A17] and compared with volumes tabulated by Cristy and Eckerman [A15]. This would detect gross geometry errors in the definition of cells.

(ii) The whole phantoms were irradiated and particles lost through errors in geometry definition were traced.

(iii) The phantom implementations were visually inspected with the plotting facility in MCNP. Surfaces that had been incorrectly implemented would be automatically highlighted.

(iv) A set of calculations for conventional abdominal, chest and head X-ray projections was performed and resulting normalized organ doses were compared with those from previous calculations based on the family of geometric phantoms [A26]. This provided validation of the implementation of the mathematical phantoms.

(v) Normalized organ doses for CT exposures were compared with previously published datasets that contain doses for the same three scanner types for the adult phantom [A8, A26]. This provided validation of the X-ray source description including the energy spectrum, filtration (flat and shaped), collimation and the random sampling of line sources. It also provided checks on the semi-automated procedures for creating and running large numbers of MCNP simulations and the normalization applied to organ doses.

A1.7 Variance reduction

Variance reduction is the term used to describe techniques that may be employed in Monte Carlo modelling to optimize the amount of useful information that is provided by a fixed number of particle histories. The most commonly used variance reduction methods are perhaps source biasing, where photons travelling in a certain direction from the source are given an increased probability weighting, and geometry splitting, where photons crossing specified geometrical surfaces are split into two or more photons whose probability weightings add up to that of the original photon. The ultimate purpose of these probability ''games'' is to ensure that the proportion of computer time that is spent following useful particle histories is maximized.

Both source biasing and geometry splitting were investigated for this problem, but it was found that neither offered any significant advantage. The scope for geometry splitting was limited owing to the fact that energy deposition is tallied over virtually the whole phantom. With respect to source biasing, it was concluded that the convenience of the adopted source description outweighed the small reduction in computing time that a biased source might produce. The

adopted figure of 250 000 histories per slice gives random errors of typically less than 5% (standard error) in the doses for organs directly in the beam. Of course, random errors in the normalized organ doses for a typical scan will be significantly less than this, since the doses from more than one slice are combined.

A2 Results

Organ absorbed doses, normalized to absorbed dose to air (or air kerma) on the scanner axis of rotation, have been computed for 1 cm transverse slices, beginning at 50 cm below the bottom of the trunk and continuing to the top of the head, for the six phantoms and three scanners in the study, i.e. 18 data sets. For the purpose of this paper, these data have been summed to give the effective doses from contiguous scanning of four regions of the body. These regions are described as trunk, abdomen and pelvis, chest, and head and neck. The boundaries of these regions correspond, in ascending order along the z-axis, to the bottom of the trunk, the bottom of the lungs, the top of the trunk and the top of the head (Table A2). They are taken to the nearest 1 cm slice boundary.

Table A2 Positions of scan boundaries for body regions in geometric phantoms relative to the base of the trunk

Region	Scan boundaries as distance (cm) along the z-axis in each phantom					
	Newborn	1 year	5 years	10 years	15 years	Adult
Trunk	0–22	0–31	0–41	0–51	0–63	0–70
Abdomen and pelvis	0–13	0–19	0–25	0–32	0–39	0–43
Chest	13–22	19–31	25–41	32–51	39–63	43–70
Head and neck	22–39	31–50	41–65	51–75	63–90	70–95

A2.1 Normalized effective dose to adults

Effective doses for adult patients, normalized to air kerma on the scanner axis of rotation, are given for the four scan regions and the three scanners in Table A3, with estimates of the statistical errors arising from the Monte Carlo method. These figures show considerable variation in normalized effective dose between scanners for the same scans, ranging up to a factor of 2 for a scan of the trunk. This is consistent with the findings of a previous study carried out for 27 scanners and an adult geometric phantom by Jones and Shrimpton [A8, A9], which included the three scanners featured in this paper.

Normalized effective dose for scans of the chest and abdomen and pelvis are, respectively, approximately factors of three and five times greater than that for a scan of the head and neck, owing to the higher concentration of radiosensitive tissues in the torso. Effective dose to the trunk is approximately the sum of the effective doses to the chest and the abdomen and pelvis.

Table A3 Values of normalized effective dose (μSv mGy^{-1}) by scanner model for standard examinations on adult patients, with random errors from Monte Carlo calculations

Scanner model	Normalized effective dose by standard examination			
	Head and neck	Chest	Abdomen and pelvis	Trunk
Siemens DRH	61±0.8	200±0.7	350±1.6	550±1.8
GE 9800	44±0.8	100±0.5	170±1.7	270±1.8
Philips LX	57±0.8	170±0.7	300±1.6	450±1.7

TABLE A4 Ratios of normalized effective dose for standard scans on adult patients in this study, $_nE_K$, and from the work of Jones and Shrimpton [A8, A9] and Hart et al [A26] $_nE_J$

Scanner model	Ratio of $_nE_K$:$_nE_J$ by standard scan			
	Head and neck	Chest	Abdomen and pelvis	Trunk
Siemens DRH	1.05	0.90	0.98	0.97
GE 9800	1.08	0.90	0.95	0.92
Philips LX	1.05	0.96	1.00	0.98

It should be stressed that the errors quoted in Table A3, which are well below 1% of normalized effective dose, are only the random errors generated by the Monte Carlo simulations, and they do not reflect the much larger potential uncertainties present elsewhere in the calculations, such as those in the anatomical modelling of the phantom and in the description of the photon spectrum. It is concluded from the smallness of these statistical errors that the use of 250 000 particle histories for each 1 cm slice is quite adequate for the purposes of this study.

Normalized effective doses for the four standard scans for the adult were compared under similar conditions with results from the earlier study of Jones and Shrimpton [A8, A9] using the program CTDOSE [A27]. As shown in Table A4, the results agree to within 10% with the most significant differences occurring for head and neck and chest scans.

A2.2 Normalized effective dose and patient age

Normalized effective doses calculated for the age-specific phantoms are plotted relative to the normalized doses for the adult phantom in Figures A3–6 as a function of phantom age, with age 20 years attributed to the adult phantom. It can be seen that the normalized effective dose to children relative to the adult can vary considerably between scanner models, but in all cases doses to small children are greater than doses to adults. The enhancement of the dose to the child is greatest for scans of the head and neck. Further, the enhancement is greatest for the GE 9800 scanner; therefore normalized dose to the newborn from a head and neck scan with the GE 9800 scanner is approximately 2.5 times that for the adult. Head and neck scans with the Philips and Siemens scanners produce relative normalized doses that are only marginally less; both being

approximately 2.2 times the adult dose for the newborn. Apart from the case of the newborn, the ratio of paediatric to adult normalized dose appears to follow a similar trend with respect to age for all three scanners for head and neck scans, as shown in Figure A3.

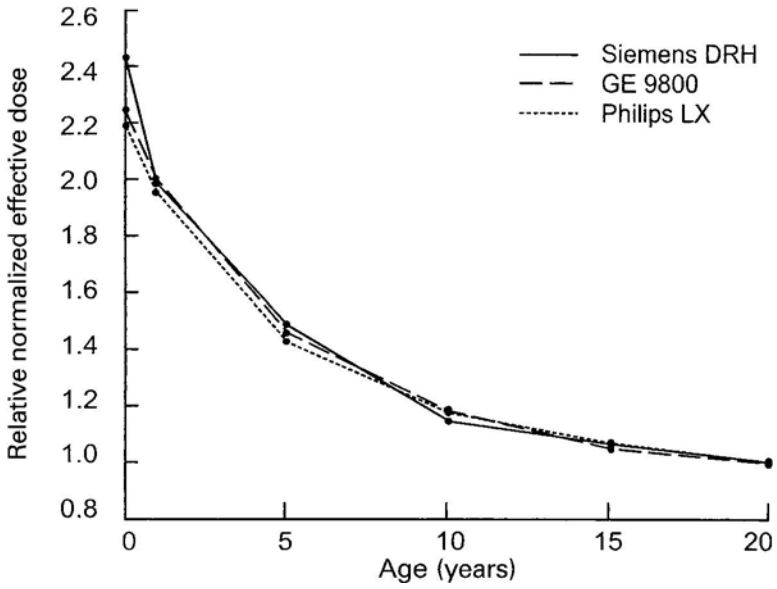

FIGURE A3 Trends with age in normalized effective dose for examination of the head and neck.

The trends in normalized dose with respect to age for scans of the chest, abdomen and pelvis, and trunk show wider variations between the scanners, as seen in Figures A4–6. For scans of the trunk, normalized dose to the newborn ranges from approximately 2.4 times the adult normalized dose for the GE 9800 scanner to only 1.3 times for the Siemens DRH scanner. The relative normalized doses appear to vary smoothly with age, with that for the 15-year-old being virtually the same as that for the adult for the Siemens scanner, and only 15% different for the GE 9800 scanner.

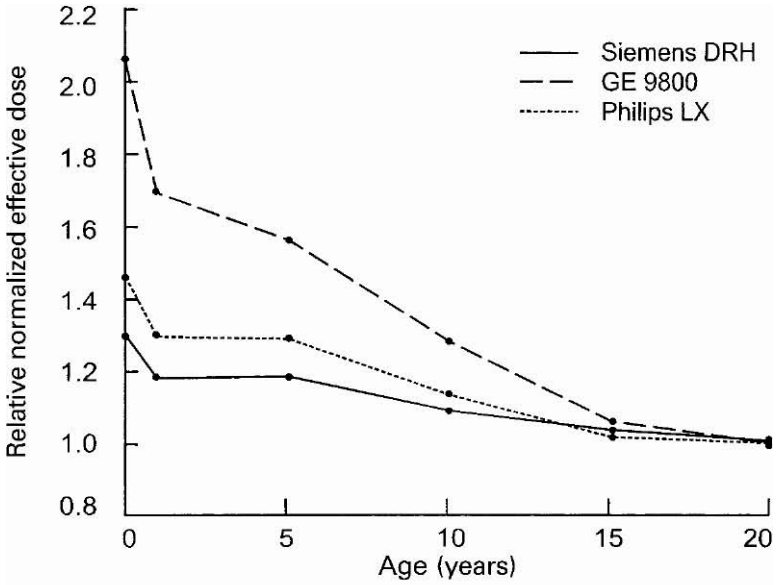

FIGURE A4 Trends with age in normalized effective dose for examination of the chest.

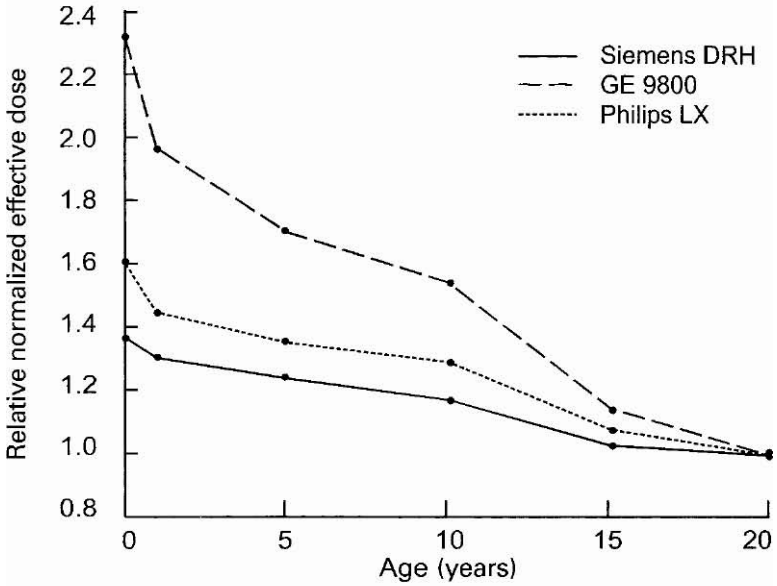

FIGURE A5 Trends with age in normalized effective dose for examination of the abdomen and pelvis.

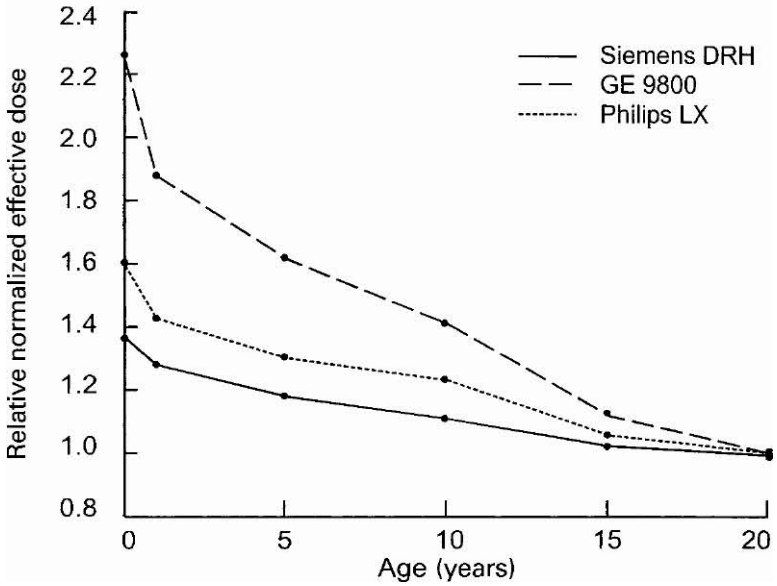

FIGURE A6 Trends with age in normalized effective dose for examination of the trunk.

The absolute value of the effective dose for a paediatric examination may be obtained by multiplying the normalized effective dose to the adult given in Table 3 by the CTDI free-in-air on the axis of rotation for the scanner, and by the ratio of the normalized paediatric dose to that of the adult (Figures A3–6). Illustrative absolute effective doses for chest scans are shown in Table A5, using typical CTDI per mAs values [A28] and typical mAs values for adult patients from a national survey of CT practices in 1989 [A29]. These figures indicate that the highest absolute effective dose to the adult (10.8 mSv) is delivered by the Philips LX scanner, while the highest dose to the newborn (17.1 mSv) is delivered by the GE 9800 scanner. Doses from these two scanners are higher than doses from the Siemens scanner for all ages, being approximately a factor of two higher for small children. It should be emphasized, however, that these are illustrative figures only, since mAs settings and scan limits are at the discretion of the user, and it has been assumed that the same tube voltage and mAs values as used on adults have been used on children.

TABLE A5 Illustrative effective doses for chest examinations on adult and paediatric patients

Scanner model	CTDI mGy mAs^{-1}	mAs	Effective dose by age in years (mSv)					
			Adult	15 y	10 y	5 y	1 y	Newborn
Siemens DRH	0.128	230	6.0	6.3	6.6	7.1	7.1	7.8
GE 9800	0.26	320	8.3	8.8	10.6	13.0	14.1	17.1
Philips LX	0.192	330	10.8	11.1	12.2	13.9	14.1	15.8

CTDI, CT dose index.

A3 Discussion

A3.1 Trends in normalized effective dose with respect to age

Figures A3–6 show a strong inverse correlation between age, and hence the size of the patient, and normalized effective dose for all the scans considered in this study. This observation is generally in agreement with results reported by Huda et al [A14] that for CT exposures of a homogeneous cylindrical phantom, mean dose to the phantom normalized to air kerma also decreases as the radius of the phantom increases. The results given here, however, go further than simply establishing a relationship between mean absorbed dose and the radius of a cylindrical phantom, in that efforts have been made to reflect the differential rates of growth for the various anatomical regions of the phantoms, and indeed for the radiosensitive organs that are used to calculate effective dose.

It should be appreciated that the tissue weighting factors used to calculate effective dose are taken to be independent of age [A30], which may be unrealistic. Effective dose has to be combined with risk factors in order to estimate health detriment, and various authors have estimated risk factors to be significantly greater for children than adults [A5, A31]. These considerations

imply that the increase in radiation risk for CT scans on children compared with adults will be even greater than the increase in effective dose.

A3.2 Trends between scanners

Measurements of the HVL of the X-ray beam on the scanner axis of rotation (see Table A1) suggest that there are only small differences in the ''hardness'' of the photon spectra from the three scanners after passage through the central region of the shaped filters. However, there is a factor of two spread in normalized effective dose (Table A3), with the Siemens DRH scanner giving the highest normalized dose and the GE 9800 scanner the lowest. The most likely cause of this difference is the presence of the shaped filter in the GE scanner, which will have the effect of reducing photon fluence in the X-ray fan beam off the scanner axis of rotation. For a head scan, for which the irradiated volume is relatively small and centred on the scanner axis of rotation, there will be a fairly uniform radiation field across the head of the child and adult phantoms for all three scanners. Hence, curves in Figure A3 for the three scanners are close to each other. However, for scans of the trunk, where the photon fluence in the X-ray fan beam will fall off significantly at greater distances from the axis of rotation for the two scanners with shaped filters, there is a greater spread between the three scanners in the normalized effective doses for child relative to adult (Figures A4–6).

Consequently, the ratio of normalized effective dose for a paediatric head and neck scan, relative to that for an adult, appears to be largely independent of the CT machine: thus the average of the three curves given in Figure A3 may, with sensible caution, be taken as a guide for most scanners. For paediatric and adult scans of the trunk, there is greater variation between scanners in the age dependence of normalized effective dose, and it may be advisable to use scanner-specific data when estimating effective doses to children.

The examples of absolute effective doses for chest scans given in Table A5 show that, when comparing scanners, the normalized effective doses given in Table A3 bear no simple relationship to the effective doses received by patients in real examinations. Indeed, the scanner that gives the highest normalized effective dose to the adult, the Siemens DRH, gives the lowest absolute effective dose for the exposure conditions assumed in Table A5. The scanner that gives the lowest normalized dose to the adult, the GE 9800, gives the highest absolute dose to the newborn for the present analysis. The values of effective dose are in the range 6–17 mSv, confirming that substantial doses are received by patients during CT examinations of the chest. Similar estimates of dose were obtained for the other three scan regions, but have not been tabulated here since the regions do not correspond so closely to those used in common clinical practice. However, it is noted that effective doses from scans of the lower trunk can be significantly higher than for the chest. For example, effective doses for scans of the entire abdomen and pelvis of the newborn could, under particular circumstances, be in excess of 35 mSv if scan protocols have not been optimized for the newborn patient.

A3.3 Comparisons with previous NRPB data

Comparisons were made with the published organ dose data for CT of Jones and Shrimpton [A8, A9], which were converted to effective doses for adults normalized to air kerma for the three scanners featured here. Jones and Shrimpton [A8, A9] did not calculate air kerma, but rather calculated energy deposition within a 0.5 cm diameter volume of muscle, centred on the scanner axis of rotation, with the same axial length (0.5 cm) as the CT beam slice. In this study, energy deposition was tallied over the whole volume of a 10 cm long column of air with a diameter of 0.5 cm, to reflect more accurately the dimensions of the pencil ionization chambers commonly used in CT dosimetry. These two different methods of tallying energy deposition result in a difference of only approximately 2% when both are converted to air kerma.

It is thought that most of the remaining differences for head and neck scans and chest scans shown in Table A4 are accounted for by the different implementations of the oesophagus and thyroid, which affect how much of these organs are irradiated in each scan. In this study the oesophagus is modelled as a straight cylindrical tube that lies in both the head and neck region and the chest region of the phantom, while for effective dose calculations using the Jones and Shrimpton data [A8, A9], the thymus was taken as a surrogate for the oesophagus and is entirely in the chest region. Hence the contribution from oesophagus to the normalized effective dose for head and neck is higher in this study in comparison with Jones and Shrimpton, while it is lower for chest. Thus for a head and neck scan with the Siemens DRH scanner, the normalized absorbed dose to the oesophagus is 12 times higher in this study than it was using data from Jones and Shrimpton, and it presently contributes approximately 10% to normalized effective dose. Correspondingly, for a chest scan, absorbed dose to the oesophagus is only 60% of that utilizing data from Jones and Shrimpton, and presently contributes approximately 10% to effective dose. The other methodological differences between the studies do not impact significantly on normalized effective dose, but can have a larger effect on individual organ doses.

To conclude, once the above effects are taken into account, the agreement with earlier NRPB data is remarkably good, which validates the descriptions of the photon fields used in the Monte Carlo simulations. Likewise, comparisons with previous NRPB data for normalized effective dose for conventional X-ray examinations show good agreement (A Khursheed, personal communication).

A3.4 Comparisons *w*ith other published data

There are few published data concerning organ and effective doses for paediatric CT from measurements [A12, A13] or calculation [A11, A14, A32–35] and none previously for the complete family of geometric phantoms. Comparisons of dose coefficients are confounded by differences not only in the phantoms and scanner models used, but also the scan lengths assumed for standard examinations. However, the present normalized dose data are in broad agreement, with due account of likely differences in conditions of exposure, with Monte Carlo

calculations for voxel paediatric phantoms by Zankl et al [A32] and Caon et al [A11].

Huda et al [A14] have already predicted increases in normalized effective dose with decreasing patient size for typical scan protocols using a GE Advantage Hi Speed scanner. At constant tube voltage and mAs settings, the dose to a newborn patient was, according to Huda et al, larger than that to an adult by factors of 2.3 for abdomen examinations and 5.3 for head examinations. The explicit results for the newborn and adult geometric phantoms in this paper indicate corresponding factors for the three scanners considered in the range 1.4 to 2.3 for scans of the abdomen and pelvis (Figure A5), and factors of 2.2 to 2.4 for the head and neck (Figure A3). The trend in normalized dose with age for abdominal scans, shown in Figure A5, appears broadly consistent with that predicted by Huda et al [A14], whereas the trend shown in Figure A3 for head and neck scans is much less pronounced than that suggested by Huda et al. It should be appreciated that there are differences in both the scan lengths and the absolute values of normalized effective dose between the study of Huda et al and the present work, which might help to explain some of this apparent discrepancy. Further analyses of these results are in progress. However, both studies clearly indicate the significant increases in patient dose, particularly to the newborn, when children are scanned using the same mAs and tube voltage settings as for adults. There is a clear need to develop size-specific protocols for paediatric CT, optimized to provide adequate image quality for the lowest dose [A35–38].

A4 Conclusions

Monte Carlo simulations of CT examinations have been performed for three scanner models for a family of six mathematical phantoms. Effective doses normalized to axial air kerma have been calculated for scans of the head and neck, chest, abdomen and pelvis, and trunk. It is shown that normalized effective doses to paediatric patients are significantly greater than doses to adult patients for all three of the scanners featured in this study. The enhancement is greatest for head and neck scans, where it is in the range 2.2–2.5 for the newborn for all three scanners. For scans of the whole trunk it ranges from 1.3 for the scanner without a shaped filter, the Siemens DRH, to 2.4 for the GE 9800 scanner.

Coupled with higher lifetime radiation risk factors for paediatric patients, the results of this study confirm that CT potentially poses significantly greater radiation risks to children than to adults. It is concluded that special efforts should be made in clinical practice to reduce doses to paediatric patients from CT by the use of size-specific scan protocols for optimized imaging.

A5 References

A1. Hart D, Wall BF. Collective dose to the UK population from medical and dental x-ray examinations. Document NRPB-R334. Chilton, UK: National Radiological Protection Board 2001.

A2. United Nations Scientific Committee on the Effects of Atomic Radiation. Sources and effects of ionizing radiation. UNSCEAR 2000 Report to the General Assembly, with Scientific Annexes. UN Sales Publication E.00.IX.3. New York: United Nations, 2000.

A3. Mettler FA, Weist PW, Locken JA, Kelsey CA. CT scanning: patterns of use and dose. J Radiol Prot 2000;20:353–9.

A4. National Radiological Protection Board. Estimates of late radiation risks to the UK population. Documents of the NRPB 1993;4.

A5. Brenner DJ, Elliston CD, Hall EJ, Berdon WE. Estimated risks of radiation-induced fatal cancer from pediatric CT. AJR 2001;176:289–96.

A6. Donnelly LF, Frush DP. Fallout from recent articles on radiation dose and paediatric CT. Pediatr Radiol 2001;31:338.

A7. Zankl M, Panzer W, Drexler G. The calculation of dose from external photon exposures using reference human phantoms and Monte Carlo methods. VI. Organ doses from computed tomography examinations. GSF-Bericht 30/91. Munich, Germany: GSF, 1991.

A8. Jones DG, Shrimpton PC. Survey of CT practice. Part 3: normalised organ doses calculated using Monte Carlo techniques. Document NRPB-R250. Chilton, UK: National Radiological Protection Board, 1991.

A9. Jones DG, Shrimpton PC. Normalised organ doses for X-ray computed tomography using Monte Carlo techniques. Document NRPB-SR250. Chilton, UK: National Radiological Protection Board, 1993.

A10. Zankl M, Panzer, Drexler G. Tomographic anthropomorphic models. Part II organ doses from computed tomographic examinations in paediatric radiology. GSF-Bericht 30/93. Munich, Germany: GSF, 1993.

A11. Caon M, Bibbo G, Pattison J. Monte Carlo calculated effective dose to teenage girls from computed tomography examinations. Radiat Prot Dosim 2000;90:445–8.

A12. Axelsson B, Persliden J, Schuwert P. Dosimetry for computed tomography examinations of children. Radiat Prot Dosim 1996;64:221–6.

A13. Giacco G, Cannata V, Furetta C, Santopietro F, Fariello G. On the use of paediatric phantoms in the dose evaluation during computed tomography (CT) thorax examinations. Med Phys 2001;28:199–204.

A14. Huda W, Atherton JV, Ware DE, Cumming WA. An approach to the estimation of effective radiation dose at CT in paediatric patients. Radiology 1997;203:417–22.

A15. Cristy M, Eckerman KF. Specific and absorbed fractions of energy at various ages from internal photon emitters. I. Methods. ORNL/TM-8381/VI. Oak Ridge, TN: Oak Ridge National Laboratory, 1987.

A16. Shrimpton PC, Edyvean S. CT scanner dosimetry. Br J Radiol 1998;71:1–3.

A17. Briesmeister JF, editor. MCNP—a general Monte Carlo N-particle transport code—version 4B. Los Alamos National Laboratory Report, LA-12625-M, 1997.

A18. Bielajew AF, Hirayam H, Nelson WR, Rogers DWO. History, overview and recent improvements to EGS4, National Research Council of Canada Report PIRS-0436, 1994.

A19. Zankl M, Petoussi N, Drexler G. Effective and effective dose equivalent—the impact of the new ICRP definition for external photon irradiation. Health Phys 1992;62:395–9.

A20. Shope TB, Gagne RM, Johnson GC. A method for describing the doses delivered by transmission x-ray computed tomography. Med Phys 1981;8:488–95.

A21. Lewis MA, Edyvean S, Sassi SA, Kiremidjian H, Keat N, Britten AJ. Estimating patient dose on current CT scanners: results of the ImPACT CT dose survey. Rad Magazine 2000;26:17–8.

A22. Cranley K, Gilmore BJ, Fogerty GW, Desponds L. Catalogue of diagnostic spectra and other data. Report No. 78. York, UK: Institute of Physics and Engineering in Medicine, 1997.

A23. Iles WJ. The computation of bremsstrahlung X-ray spectra over an energy range 15 keV to 300 keV. Document NRPB-R204. Chilton, UK: National Radiological Protection Board, 1987.

A24. Jones DG, Wall BF. Organ doses from medical X-ray examinations calculated using Monte Carlo techniques. Document NRPB-R186. Chilton, UK: National Radiological Protection Board, 1985.

A25. Wall BF, Harrison RM, Spiers FW. Patient dosimetry techniques in diagnostic radiology. Report No. 53. York, UK: Institute of Physical Sciences in Medicine, 1988:28–39.

A26. Hart D, Jones DG, Wall BF. Coefficients for estimating effective doses from paediatric X-ray examinations. Document NRPB-R279. Chilton, UK: National Radiological Protection Board, 1996.

A27. Le Heron JC. CTDOSE (PC program). Christchurch, New Zealand: National Radiation Laboratory, 1993.

A28. ImPACT. St George's Hospital, London. http:// www.impactscan.org

A29. Shrimpton PC, Jones DG, Hillier MC, Wall BF, Le Heron JC, Faulkner K. Survey of CT practice in the UK. Part 2: dosimetric aspects. Document NRPB-R249. Chilton, UK: National Radiological Protection Board, 1991.

A30. ICRP. 1990 Recommendations of the International Commission on Radiological Protection. Publication 60. Ann ICRP 1991;21. Oxford, UK: Pergamon, 1991.

A31. National Radiological Protection Board. Occupational, Public and Medical Exposure. Documents of the NRPB 1993;4.

A32. Zankl M, Panzer W, Petoussi-Henss N, Drexler G. Organ doses for children from computed tomography. Radiat Prot Dosim 1995;57:393–6.

A33. Ware DE, Huda W, Mergo PJ, Litwiller AL. Radiation effective doses to patients undergoing abdominal CT examinations. Radiology 1999;210: 645–50.

A34. Huda W, Scalzetti EM, Roskopf M. Effective doses to patients undergoing thoracic computed tomography examinations. Med Phys 2000;27:838–44.

A35. Huda W, Chamberlain CC, Rosenbaum AE, Garrisi W. Radiation doses to infants and adults undergoing head CT examinations. Med Phys 2001; 28:393–9.

A36. Huda W, Scalzetti EM, Levin G. Technique factors and image quality as functions of patient weight at abdominal CT. Radiology 2000;217:430–5.

A37. Chan C-Y, Wong Y-C, Chau L-F, Yu S-K, Lau P-C. Radiation dose reduction in paediatric cranial CT. Pediatr Radiol 1999;29:770–5.

A38. Donnelly LF, Emery KH, Brody AS, Laor T, Gylys-Morin VM, Anton CG, et al. Minimizing radiation dose for paediatric body applications of single-detector helical CT. AJR 2001;176:303–6.